

A NUMERICAL INVESTIGATION OF HEAD WAVES AND LEAKY MODES IN FLUID-FILLED BOREHOLES

by

Frederick L. Paillet
U.S. Geological Survey
Denver, CO 80225

and

C.H. Cheng
Earth Resources Laboratory
Department of Earth, Atmospheric, and Planetary Sciences
Massachusetts Institute of Technology
Cambridge, MA 02139

ABSTRACT

Although synthetic borehole seismograms routinely can be computed for a wide range of borehole conditions, the physical nature of shear and compressional head waves in fluid-filled boreholes is poorly understood. This paper presents a series of numerical experiments designed to provide insight into the physical mechanisms controlling head wave propagation in boreholes. These calculations demonstrate the existence of compressional normal modes equivalent to shear normal modes, or pseudo-Rayleigh waves, with sequential cutoff frequencies spaced between the cutoff frequencies for the shear normal modes. Major contributions to head wave spectra are shown to occur in discrete peaks at frequencies just below mode cutoff for both compressional and shear modes. This result is confirmed by calculations with synthetic waveforms at frequencies corresponding to mode cutoff, and by branch cut integrals designed to yield independent spectra for the compressional mode. In the case of soft formations where shear velocity falls below acoustic velocity in the borehole fluid, leaky compressional normal modes attain properties similar to those observed for shear normal modes in the hard rock case. This result is formally related to a fluid-fluid waveguide with undamped compressional normal modes in the limit of vanishing shear velocity. Synthetic waveforms demonstrate that high amplitude arrivals, traveling at velocities less than the acoustic velocity of the borehole fluid, and at frequencies above a few kilohertz represent the Airy phase of the compressional mode and not a tube wave. Comparison of synthetic waveforms with waveforms obtained in soft sea sediments indicates that the predicted Airy phase arrivals are present in the experimental data.

INTRODUCTION

Acoustic well logs have been used for decades in geological exploration. The conventional acoustic transit-time log provides reliable measurements of the effective compressional velocity of saturated rocks. Most practical references on borehole technology treat the first arrivals in borehole waveforms as simple compressional body waves (Guyod and Shane, 1969; Pickett, 1960). However, theoretical analysis shows that the measured arrivals represent critically refracted

waves traveling along the borehole wall. Although the cylindrical geometry of the borehole wall complicates the problem, Peterson (1974) showed that the compressional and shear head waves in boreholes arise from the same branch cut contributions to the Fourier integral that account for the head waves at plane interfaces, as calculated by Ewing et al., (1957). This theory appears especially complicated in many cases because the early literature used an asymptotic method (saddle-point integration) to approximate waveform solutions at large source-to-receiver separations. Almost all of this mathematical theory fortunately has proven irrelevant to the practical well logger because the analysis consistently shows that first acoustic arrivals travel at compressional velocity. In those cases where one is concerned with such details as effective wave penetration into the borehole wall, acoustic fullwave models can be used numerically to calculate the effects of concentrically layered media on the composite waveform (Tubman et al., 1984; Baker, 1984).

In recent years many attempts have been made to extract other information from acoustic waveform data in addition to compressional velocities. Investigators most often have sought attenuation and shear velocity (Cheng et al., 1982; Willis and Toksöz, 1983). Results have not been encouraging, and investigators have repeatedly attributed the problem to the physical nature of head waves in boreholes. Several recent investigations attempted to use the synthetic waveform calculations for various seismic velocities and borehole conditions to provide a quantitative relation between rock properties and waveform parameters (Cheng and Toksöz, 1981; Paillet and White, 1982; Baker, 1984). This approach served to highlight the complex nature of the dependence of head-wave dispersion and attenuation on borehole conditions. In using this approach, the complexity of the mathematical theory is in itself a major obstacle to understanding. Additional physical insight into the mechanism of head-wave propagation along boreholes is clearly needed.

This report describes a series of numerical experiments designed to provide a clear understanding of the mechanism of compressional and shear head-wave propagation along fluid-filled boreholes. The emphasis is placed on identifying those factors that contribute to observed compressional and shear arrivals under conditions appropriate for realistic well-logging situations. These conditions include two primary geometrical constraints: (1) borehole diameters less than seismic and acoustic wavelengths, and (2) source-receiver separations ranging from 1 to 10 acoustic wavelengths. Seismic velocities of interest range from the velocities of hard crystalline rock (where shear velocity is much greater than acoustic velocity in the borehole fluid) to the velocities of softer and more plastic argillaceous sediments (where compressional velocity is greater than acoustic velocity in the borehole fluid, and shear propagation may be negligible). In terms of practical numerical calculations, two ratios of interest exist: the ratio of compressional to shear velocity (i.e., Poisson's ratio) and the ratio of shear velocity to acoustic velocity in the borehole fluid.

In the first section of this paper, we will review briefly the mathematical theory of borehole waveform calculations. In a subsequent section, we will use the numerical evaluation of the Fourier-inversion integral to identify those frequencies and wave numbers that contribute to head-wave integrals. A following section then will illustrate how this insight into head-wave amplitude spectra can be used to predict the character of head waves in the composite spectrum. A major result will be the identification of scaling laws that relate the observed properties of head waves to borehole geometry and seismic velocities. Then a final section will deal

with the special case of "slow formations" where more plastic rocks tend to have low shear velocities and high Poisson's ratios. Special emphasis will be placed on identifying the formal limit at which shear velocity vanishes, and the borehole becomes a liquid-liquid waveguide. Several of the properties of such waveguides will be shown to have general application to soft sediments encountered in well logging.

NUMERICAL THEORY

The equations for acoustic propagation along a fluid-filled borehole were originally formulated by Biot (1952), and extended to the borehole with centralized logging tool by White and Zechman (1968). Peterson (1974), Rosenbaum (1974), Tsang and Rader (1979) and Cheng and Toksöz (1981) subsequently have examined the theory in greater detail. The wave propagation problem formulated in these references assumes axial symmetry, and restricts the possible solutions by the usual radiation condition (outward propagating waves only). The formal solution can be expressed in the form:

$$p(r,z,t) = \frac{1}{(2\pi)^2} \int_{-\infty}^{\infty} \int_{-\infty}^{\infty} S(l,\omega) P(l,\omega) e^{ilz} e^{i\omega t} dl d\omega \quad (1)$$

where $p(r,z,t)$ denotes the measured pressure at the surface of the logging tool ($r=R$) at a specified distance uphole from the acoustic energy source ($z=Z_0$); l is the axial wavenumber and ω is the acoustic frequency. $S(l,\omega)$ and $P(l,\omega)$ represent transforms of the source and delta function response of the borehole. The transform $P(l,\omega)$ hereafter will be referred to as the pressure response function for the borehole. In the analysis given by Peterson (1974), the pressure function is represented further as the ratio of two functions:

$$P(l,\omega) = N(l,\omega) / D(l,\omega) \quad (2)$$

The denominator in (2) gives the location of the singularities that sometimes correspond to sharp amplitude peaks in frequency spectra for the inverted waveform.

The inversion integral (1) usually is integrated first with respect to wavenumber, yielding the effective response of the borehole to forcing at a single harmonic frequency, $f = \frac{\omega}{2\pi}$. This spectrum then is multiplied by the source frequency spectrum to yield response of the borehole to forcing by a source of finite bandwidth. A major complication in numerical evaluation of (1) is the presence of branch cuts associated with the complex square roots:

$$m_1 = (l^2 - \frac{\omega^2}{V_f^2})^{1/2} ; m_2 = (l^2 - \frac{\omega^2}{V_p^2})^{1/2} ; \text{ and } k = (l^2 - \frac{\omega^2}{V_s^2})^{1/2} \quad (3)$$

that appear in the representation of $P(l,\omega)$. The quantities m_2 and k introduce branch cuts into the complex wavenumber plane because radiation conditions formally restrict the specific choice of sign allowed in taking the square root in (3). No such branch point is associated with m_1 , because both inward and outward

propagating wave solutions are retained in the borehole fluid, and both signs of the square root are always selected.

A second complication is the presence of singularities corresponding to the zeros of $D(l,\omega)$ in (2) that lie along the integration path implied by (1). White and Zechman (1968) and Peterson (1974) approached this problem by calculating separately the contributions from these wavenumbers according to residue theory. Other investigators adopted the more effective approach of introducing numerical damping into the calculation (Rosenbaum, 1974; Cheng and Toksöz, 1981), which is equivalent to the use of a conversion factor in improving the convergence properties of the Fourier integral in (1) (Morse and Feshbach, 1953).

The singularities lying along the real wavenumber axis have been shown to correspond to undamped modes of wave propagation along the borehole. One of these singularities occurs at a characteristic velocity slightly less than acoustic velocity in the borehole fluid, and is closely allied to the Stoneley mode of propagation along a plane interface (Biot, 1952). This so called tube wave is only slightly dispersive for hard, crystalline rocks. For rocks with $V_s > V_f$, one or more singularities, corresponding to propagation with phase velocities lying between shear and fluid velocities, can also exist. These modes correspond to multiple internal reflections of acoustic-wave energy during propagation along the borehole waveguide. Unattenuated propagation requires total internal reflection, which depends upon critical angle of shear refraction and annulus width. Only a few such modes (at most) are possible at a given frequency under typical logging conditions. The phase velocities of these multiply-reflected modes decrease significantly with increasing frequency above cutoff, so the modes are highly dispersive. These nodes are commonly known as shear normal modes (Paillet and White, 1982), pseudo-Rayleigh waves (Cheng and Toksöz, 1981), or reflected conical waves (Biot, 1952). The large acoustic wavelengths with respect to borehole radius also indicate that guided waves provide substantial penetration into the borehole wall during reflection. Paillet and White (1982) showed that the shear normal modes formally decouple into internally reflected waves and Rayleigh wall waves in the limit of vanishing fluid density. Therefore, shear normal modes represent the hybridization of surface waves in the solid and internally reflected fluid waves at the relatively long wavelengths typical of borehole logging.

In addition to the finite set of undamped shear normal modes, an infinite set of leaky shear modes exist corresponding to all possible multiple reflections in which total internal reflection does not occur, and shear radiation therefore "leaks" away from the borehole. These modes correspond to singularities lying off the real wavenumber axis. Therefore they contribute to the inversion integral even when those modes lying on the real axis are removed by the method of White and Zechman (1968). In almost all cases relevant to acoustic logging, these modes lie so far away from the path of integration on the real wavenumber axis that the contribution to the inversion integral is negligible.

Although not normally discussed in the borehole-waveform literature, leaky compressional modes also exist. These modes appear highly attenuated in hard, crystalline rocks. They become important in the limit of vanishing shear velocity as the borehole becomes a liquid-liquid waveguide. Several authors have used the analogy between shear normal modes and compressional normal modes in the two liquid cases to simplify the mathematics of mode theory (Jacobi, 1949; Rosenbaum, 1960; Aki and Richards, 1980). Phinney (1961) describes in detail the physical

properties of leaky compressional (or PL) wave modes in an ocean layer overlying soft sediments. Cheng and Toksöz (1981) observed that compressional head waves appeared prolonged in synthetic borehole seismograms for rocks with Poisson's ratios greater than .35. They concluded that a significant PL-mode contribution was present in such cases, and could be used to infer Poisson's ratio in practical situations where shear velocities could not be measured directly.

COMPRESSIVE AND SHEAR HEAD WAVES IN HARD ROCKS

Almost all of the existing literature on the theory of head waves in boreholes treats the case of a water-filled borehole penetrating a hard crystalline rock such as sandstone. Here we are referring to the case of seismic velocities where both V_p and V_s are greater than V_f , with Poisson's ratio of 0.25. To illustrate examples, we shall use the typical borehole parameters and seismic velocities listed under the sandstone case with centralized logging tool in Table 1. Using these values and a frequency of 25 kHz in the evaluation of the wavenumber integral in (1), we find that two shear normal-mode singularities lie on the positive real-wavenumber axis to the right of the apparent fluid branch point (Figure 1). A corresponding set of singularities is found on the negative real wavenumber axis in Figure 1, and the sign conventions used in deriving (1) indicate that these contribute residues when the inversion integral is inverted by complex integration. This is indicated in Figure 1 by the fact that only the singularities on the negative real axis are enclosed by the integration path.

The theory presented by Ewing et al. (1957) and Peterson (1974) indicates that when branch cuts are taken as shown, head-wave contributions occur from differences in pressure function evaluated on either side of the branch lines. The theory led Peterson (1974) to the conclusion that waveforms would consist of normal modes and tube waves, with head waves arising from the integration around branch cuts. Peterson noted that this rotation of branch cuts from the conventional position on the real wavenumber axis might result in the complex integration path encircling some of the leaky normal modes on the lower Riemann sheet, but Tsang and Rader (1979) demonstrated that branch-cut integrations alone can give an acceptable approximation to head waves.

The physical mechanism for the generation of head waves in boreholes penetrating hard rocks was approached by identifying those situations where large phase differences occurred along branch lines. Initially observed that such phase differences arose for very restricted values of frequency. The special frequency intervals were subsequently identified as those just below the cutoff for compressional and shear normal modes. We hereafter use "conventional" branch cuts lying along the real axis: these are the branch cuts built into the complex arithmetic routines used in almost all numerical integration schemes such as those given by Cheng and Toksöz (1981) and Rosenbaum (1974).

Trajectories of the singularities associated with compressional and shear normal modes for the sandstone case are illustrated in Figures 2 and 3. The first compressional normal mode (Figure 2) represents a leaking or damped mode above cutoff, coalesces with the branch point at cutoff, and moves away from the branch point on the lower sheet at frequencies below cutoff. The first shear normal mode is an undamped mode on the real axis above cutoff (Figure 3). Although not shown Figures 2 and 3, both compressional and shear modes possess conjugate "growing"

modes on lower sheets, formally representing modes that are tied to incoming wave energy.

The properties of leaky normal mode singularities would be of little practical interest except that the presence of leaky modes near the branch point accounts for rapid changes in $P(l,\omega)$ along the real wavenumber axis, illustrated in Figures 4 and 5. $P(L,\omega)$ along the real wavenumber axis is shown in Figure 4 for frequencies just above and below compressional normal-mode cutoff at 16.5 kHz. The character of the pressure function changes rapidly with frequency in this range. Above cutoff, $P(l,\omega)$ appears similar to a simple undamped mode; whereas a sharp cusp-shaped excursion occurs at the branch point for frequencies below cutoff. Above cutoff, the function indicates a slightly damped mode with large but continuous excursions in amplitude. Below cutoff, a finite discontinuity exists in the derivative of $P(l,\omega)$ caused by the presence of the singularity on the lower Riemann sheet near the branch point. The integration path on the upper sheet effectively sees the singularity from very different distances on either side of the branch point. This discontinuity in the derivative represents a contribution to the integral at the compressional branch point, thus contributing to the composite spectrum at exactly compressional velocity ($l_{\text{real}}/\omega = V_p$). Also note that at larger source-to-receiver separations the term e^{ilz} in (1) becomes highly oscillatory, and contributions to the wavenumber integral will be confined to intervals where $P(l,\omega)$ changes rapidly with l . In some cases, the leaky compressional mode can contribute to the total solution at frequencies above cutoff, but this wave energy will be dispersed over phase velocities slightly less than V_p . Such arrivals were observed in synthetic borehole seismograms by Cheng and Toksöz (1981).

A similar set of pressure functions in the vicinity of shear normal-mode cutoff is illustrated in Figure 5. Here head wave contributions come from the leaky mode below normal mode cutoff. An important point is that the theory provides a formal mathematical means of separating normal modes from the shear head wave; normal modes are associated with contributions from the undamped or leaky modes on the upper sheet, whereas shear head waves arise from the excursion in $P(l,\omega)$ at the branch point where leaky modes lie near the branch point on the lower sheet. An additional complication in the theory is introduced by mode amplitudes in the vicinity of mode cutoff. When modes coalesce with branch points, the associated wave motions are neither incoming nor outgoing. In this case the oscillations extend to infinity, and they would require infinite energy to excite. Therefore, energy arguments confirm the results of numerical mode tracking; mode amplitudes vanish in the limit as modes coalesce with branch points. The relative strengths of head waves, therefore, depend upon the rate at which mode amplitudes increase as singularities move away from mode cutoff. We have found that the calculations of amplitudes and damping factors (imaginary part of mode wavenumber) along with phase and group velocities are useful in predicting the character of composite waveforms.

HEAD WAVE APPLICATIONS

The theoretical considerations presented in the previous section provide several specific ways in which waveform properties can be predicted. First, the association of head waves with relatively narrow frequency bands just below mode cutoff indicates that resonances within the confined borehole fluid indirectly contribute to the head waves. The leaky modes are shown to influence directly the frequency

spectrum of the critically refracted head waves. This observation is consistent with the calculations given by Rosenbaum (1960) for critically refracted waves along two-fluid waveguides. Rosenbaum showed that head waves could be represented as either branch-cut integrals as given by Ewing et al. (1957), or as an infinite series of residues evaluated at the leaky normal modes and their conjugates. This relationship between head wave excitation and borehole fluid resonances is a fundamental property of waves in boreholes under typical logging conditions. Even when source-receiver spacings are very long, acoustic wavelengths are still larger than the width of the annulus between logging tool and borehole wall. For this reason the ratio of acoustic source wavelength to annulus width is the single most important factor in borehole waveform modeling.

One partial result of this theory is the prediction that the head waves produced in a cylindrical borehole will have a frequency spectrum composed of alternate peaks of compressional and shear energy, as shown in Figure 6. The frequency peaks can be predicted by calculating the compressional and shear-normal mode cutoff frequencies for the given set of seismic velocities and fluid annulus width. Scarascia et al. (1976) observed that the different frequency content between compressional and shear head waves in boreholes can be used to separate the two wave modes in experimental data. Multiple peaks in the head wave spectra are also indicated in the calculations given by Paillet and White (1982).

Tsang and Rader (1979) give an alternate method for computing the compressional head waves in equation (1). The method is based on integration around the compressional branch cut illustrated in Figure 1; this method has been shown to provide a satisfactory approximation to the results from the complete integration in at least some cases. The method as originally presented also used a ray expansion for the integrand in (1) in which only the first term was retained. This method deliberately was chosen to avoid the mode coalescence problem; therefore, it might have a major effect on the calculations if mode coalescence provides a major part of head wave amplitude. The amplitude spectrum produced by such a first order approximation effectively removes the fluid resonances. When higher order terms are retained in the expansion, the compressional head wave spectrum is shown to break up into multiple peaks as expected from the theory (Figures 7b and 7c).

The theory also can be tested by computing the response of boreholes to narrow band forcing at frequencies corresponding to the peaks in Figure 6. This has been done in Figure 8 for frequencies corresponding to first and second shear mode cutoffs and second compressional mode cutoffs. The calculations for forcing at shear mode cutoff frequencies (11 and 23 kHz) indicate waveforms with strong shear arrivals and weak compressional arrivals. The result at an intermediate frequency gives a waveform with higher amplitude compressional arrivals and negligible shear head waves. The compressional arrivals appear somewhat after calculated compressional head wave arrival time because the second compressional mode requires the additional fluid delay associated with two internal reflections. All three cases correspond to the sandstone case in Table 1, with a 10 cm diameter rigid logging tool in the borehole. These synthetic seismograms demonstrate the relationship between head wave excitation and mode cutoff frequencies.

Another important application of the theory is the realization that shear-energy arrivals are associated with shear normal modes or leaky shear modes. Shear head-wave spectra will not resemble the spectrum of the acoustic source; they will consist of multiple spectral peaks producing complicated interference patterns at uphole

receivers. This is illustrated by considering the effect of different borehole diameters and source frequency bands on shear-arrival identification and accuracy of shear-velocity determination. Three different magnetostrictive transducers (34, 20, and 15 kHz) were used in a 15-cm borehole in granite. Seismic velocities were already well defined by core tests and other data; they are given under the granite case in table 1. Waveforms obtained at two uphole receivers are given in Figure 9a for the highest frequency source and Figure 9b for the lowest frequency source. Results obtained with a recent shear picking algorithm (Willis and Toksöz, 1983) for a representative interval are given in Figure 9c and 9d. The shear picking routine appears to work very well with low-frequency data, but is clearly in error for high-frequency data. Arrivals were picked visually at the wave peaks indicated by the letters in Figure 9; corresponding velocities are listed in table 2. The picked shear velocities are all very close to the known value of 3.35 km/s for low-frequency data, but vary over a wide range for high-frequency data. Inspection of the waveforms indicates that a great change in overall appearance of shear arrival occur between receivers for high-frequency data. We attribute this change to the interference between two different modes subjected to different levels of attenuation in traveling a finite distance. The very regular shear arrivals in low-frequency data do not provide as well defined an indication of arrival time, but moveout between individual peaks in the data is consistently close to shear velocity.

Appearance of the borehole waveforms in Figure 9 suggests an explanation for the effectiveness of ultra-long-spaced acoustic logging tools for shear velocity logging (Koerperich, 1979). Under the constant Q approximation for attenuation in real rocks (Aki and Richards, 1980), the highest frequencies of higher modes would be subjected to higher levels of attenuation in traveling a fixed distance. Therefore, far-spaced receivers would detect waveforms in which the higher shear modes would have been attenuated, which should facilitate shear-velocity picking. These considerations indicate that the optimum waveform logging configuration would be long source receiver spacings to insure dominance of the fundamental shear mode, along with closely spaced receiver pairs to avoid the phase "wrap-around" problem.

The head wave theory indicates one additional case in which predictions readily can be verified. Relatively low head wave excitation should occur in cases where all source energy is concentrated at frequencies below cutoff for the first normal mode; an example is given in Figure 10. Synthetic seismograms for this case show that both shear and compressional arrivals have exceedingly small amplitudes. A set of experimental waveforms obtained in an 8 cm borehole in granite also show no detectable head-wave arrival (Figure 11a,b). Several waveforms were obtained in granite at higher receiver gain settings and smaller digitization intervals (Figure 11c). These waveforms show a barely detectable high-frequency arrival that may be a shear head wave. This energy may have been excited by the upper end of the source energy band; it appears to correspond with the 30 kHz cutoff for the first normal mode.

HEAD WAVES AND LEAKY MODES IN SLOW FORMATIONS

Early literature on borehole waveforms dealt almost entirely with hard formations. More recent studies have concentrated on the use of measured tube-wave velocities to determine shear velocities in rocks where V_s is much lower than V_f , as originally proposed by White (1965). However, the fact that compressional normal modes must change character as the shear velocity becomes very small is

clear. That is, borehole waveforms must approach the liquid-liquid waveguide limit as shear velocity approaches zero (Jacobi, 1949). In this limit, the compressional modes become undamped and dispersive in a manner closely analogous to the normal modes in hard formations. The compressional-mode trajectory illustrated in Figure 2 was generated for the sandstone case with rigid logging tool in Table 1. If compressional modes are to become slightly damped dispersive modes, then the trajectory above mode cutoff in Figure 2 should move towards the real axis, and mode amplitude should increase as shear velocity becomes small.

The properties of compressive modes can be investigated by plotting the mode trajectory for shale ("B") in Table 1. Amplitudes, damping factors, and group and phase velocities for the fundamental and first two compressional modes for this case are given in Figure 12. These modes exhibit phase velocities that decrease with increasing frequency, indicating that the mode trajectory has curved back towards the real wavenumber axis, rather than moving straight downward towards high damping at nearly constant phase velocity as in Figure 2. Even though shear velocity is finite, the dispersion curves bear a strong resemblance to shear normal modes. This is a general result of our calculations; compressive normal modes begin to assume the general character of shear normal modes in "slow" rocks whenever shear velocity falls below V_f .

Cheng and Toksöz (1981) demonstrated that Poisson's ratios greater than 0.35 produced significant changes in waveform character, even in "hard" rocks. The effect of Poisson's ratio on compressional modes in "slow" formations is illustrated in Figure 13. The data clearly show that the effect of increasing Poisson's ratio increases mode dispersion and amplitude, while decreasing mode damping. The dispersive nature of these compressional modes indicates that high amplitude arrivals at velocities somewhat less than V_f may be attributed to the Airy phase of a compressional mode.

Synthetic waveforms obtained using narrow band sources of 7.5, 10, 15 and 20 kHz are compared to group and phase velocities and amplitudes calculated for the fundamental compressional mode in Figure 15 (shale "A" in Table 1). The waveform calculated for 7.5 kHz represents excitation at frequencies below the Airy phase of the mode, and most of the arriving energy starts right at predicted compressional arrival time (1.2 msec). At 10 kHz most energy is arriving at 1.2 msec but changes in phase occur after 1.5 msec indicating the superposition of a slower mode. At frequencies above the group velocity minimum, mode amplitudes have become large, and the waveform is dominated by arrivals after direct fluid travel time. The large amplitudes arriving after 1.6 msec in Figure 14c apparently represent the Airy phase in the synthetic waveform. The group velocity plot for this mode indicates that energy arriving after the group velocity minimum (where mode amplitude becomes large) travels at velocities ranging from 1.3 to 1.45 km/s corresponding to arrival times from 1.7 to 2.0 msec at a source-receiver separation of 2.4 m. This interval corresponds with the largest amplitudes in Figures 14c and 14d.

Waveforms obtained in soft deep sea sediments with velocities and other parameters close to those listed for shale "B" in table 1 are given by Toksoz et al. (1985). The DSDP waveforms are compared to a synthetic seismogram for shale "B" with broad-band forcing centered on 12 kHz in Figure 15. The Airy phase in the synthetic seismogram matches the high amplitude late arrivals in the experimental data.

Properties of the tube-wave mode also change somewhat for slow formations. In the case of hard formations, Paillet and White (1982) showed that the tube-wave mode could be traced to relatively high frequencies at approximately constant amplitude. At frequencies above shear normal mode cutoff, tube-wave modes were always detectable in the model even if normal-mode amplitudes were much greater. In the case of slow formations, the tube-wave mode becomes undetectable at frequencies above 5 kHz (Figure 16). Tube-wave amplitudes have dropped so many orders of magnitude beyond the peak near 2.5 kHz that the tube-wave singularity barely can be detected at all. Tube waves cannot account for the high-amplitude late arrivals apparent in Figure 14a.

SUMMARY

Various numerical experiments involving both complete synthetic borehole seismograms and numerical calculation of individual modes indicate that the properties of compressional and shear head waves in fluid-filled boreholes are influenced greatly by the resonant conditions in the borehole fluid. The multiply-peaked spectra for head wave excitation are directly related to the narrow annulus of fluid between the nearly rigid centralized logging tool and the borehole wall. Even when source to receiver distances are made very large, the annulus width remains less than the acoustic wavelength. This is clearly an inherent property of acoustic waveform logging: the tool must never be decentralized by more than a fraction of the acoustic wavelength if signals are to be azimuthally averaged.

The theory presented here illustrates the ways in which the resonances in borehole fluid influence the observed properties of critically refracted compressional and shear head waves. The possibility that certain refracted waves can come close to exciting resonant frequencies in the borehole fluid greatly influences computed head wave spectra. Although energy arguments demonstrate that mode amplitude must vanish in the limit as compressional and shear modes coalesce with branch points at mode cutoff from above, finite mode amplitudes just below cutoff produce peaks in the shear and compressional head wave spectra. Complicated interference patterns associated with excitation of multiple head wave peaks probably can explain many of the difficulties encountered in attempts to extract shear velocities and shear and compressional wave attenuation from waveform data.

Spectral calculations also show that leaky compressional modes become especially important for "soft" sediments where Poisson ratios become greater than 0.3, and shear velocity falls below the acoustic velocity of the borehole fluid. In those cases, the borehole begins to act like a fluid-fluid waveguide, with only slightly damped compressional normal modes showing dispersion curves very similar to those calculated for shear normal modes in "hard" rocks. Mode calculations show that tube waves are effectively unexcited at frequencies above a few kHz in soft formations. Therefore the high-amplitude arrivals observed at travel times slightly greater than direct fluid travel time appear to be the Airy phase associated with the minima in group velocity calculated for these modes. This suspicion is confirmed by synthetic seismograms, and by comparison of synthetic seismograms generated with experimental waveforms for argillaceous sea sediments to experimental waveforms.

ACKNOWLEDGEMENTS

The authors would like to thank Prof. J.E. White of the Colorado School of Mines for many stimulating and constructive discussions on the subject of elastic wave propagation in a borehole, and Zhang Jinzhong of ERL and the Sian Petroleum Institute for generating the P-wave spectra shown in Figure 7. C.H. Cheng is partially supported by the Full Waveform Acoustic Logging Consortium at M.I.T. and by National Science Foundation grant No. OCE-8408761.

REFERENCES

- Aki, K., and Richards, P.W., 1980, Quantitative seismology: theory and methods, Freeman, San Francisco, 932 p.
- Baker, L.J., 1984, The effect of the invaded zone on full wave train acoustic logs: *Geophysics*, **49**, 796-809.
- Blot, M.A., 1952, Propagation of elastic waves in a cylindrical bore containing a fluid: *J. Appl. Phys.*, **23**, 997-1009.
- Cheng, C.H., and Toksöz, M.N., 1981, Elastic wave propagation in a fluid-filled borehole and synthetic acoustic logs: *Geophysics*, **46**, 1042-2053.
- Cheng, C.H., Toksöz, M.N., and Willis, M.E., 1982, Determination of *in situ* attenuation from full waveform acoustic logs: *J. Geophys. Res.*, **87**, 5477-5484.
- Ewing, W.N., Jardetsky, W.S., and Press, F., 1957, Elastic Wave in Layered Media, McGraw-Hill, New York, 357 p.
- Guyod, H., and Shane, L.E., 1969, Geophysical Well Logging, Volume 1: Introduction to Logging and Acoustic Logging, Guyod, Houston, 256 p.
- Jacobi, W.J., 1949, Propagation of sound waves along liquid cylinders: *J. Acous. Soc. Am.*, **21**, 120-127.
- Koerperich, E.A., 1979, Shear wave velocities determined from long and short spaced borehole acoustic devices, *Soc. Petr. Engr., Inst. Mining and Metall. Engr.*, paper SPE 8237, 12 p.
- Morse, P. M., and Feshbach, H., 1953, Methods of Theoretical Physics, McGraw-Hill, New York, 1978 p.
- Paillet, F.L., and White, J.E., 1982, Acoustic modes of propagation in the borehole and their relationship to rock properties: *Geophysics*, **47**, 1215-1228.
- Peterson, E.W., 1974, Acoustic wave propagation along a fluid-filled cylinder: *J. Appl. Phys.*, **45**, 3340-3350.
- Phinney, R.A., 1961, Leaking modes in the crustal waveguide, Part 1: the ocean PL wave: *J. Geophys. Res.*, **65**, 1445-1469.
- Pickett, G.R., 1960, The use of acoustic logs in the evaluation of sandstone reservoirs: *Geophysics*, **25**, 250-274.
- Rosenbaum, J.H., 1960, The long time response of a layered elastic medium to explosive sound: *J. Geophys. Res.*, **65**, 1577-1614.
- Rosenbaum, J.H., 1974, Synthetic microseismograms: logging in porous formations: *Geophysics*, **39**, 14-32.
- Scarascia, S.B., Colombi, B., and Cassinis, R., 1976, Some experiments on transverse waves: *Geophys. Prosp.*, **24**, 549-568.

- Toksöz, M.N., Wilkens, R.H., and Cheng, C.H., 1985, Shear wave velocity and attenuation in ocean bottom sediments from acoustic waveform logs: *Geophys. Res. L.*, **12**, 37-40.
- Tsang, L., and Rader, D., 1979, Numerical evaluation of the transient acoustic waveform due to a point source in a fluid-filled borehole: *Geophysics*, **44**, 1706-1720.
- Tubman, K.M., Cheng, C.H., and Toksöz, M.N., 1984, Synthetic full waveform acoustic logs in cased boreholes: *Geophysics*, **49**, 1051-1059.
- White, J.E., 1965, Seismic waves: radiation transmission and attenuation: McGraw-Hill, New York, 305 p.
- White, J.E., and Zechman, R.E., 1968, Computer response of an acoustic logging tool: *Geophysics*, **33**, 302-310.
- Willis, M.E., and Toksöz, M.N., 1983, Automatic P and S velocity determination from full waveform digital acoustic logs: *Geophysics*, **48**, 1631-1644.
- Wyllie, M.R.J., Gregory, A.R., and Gardner, G.H.F., 1958, An experimental investigation of factors affecting elastic wave velocities in porous media: *Geophysics*, **23**, , 459-493.

Table 1. Seismic velocities and borehole parameters for test cases.

Case	V_p km/s	V_s km/s	V_f km/s	R_{tool} cm	R_{hole} cm	Poisson's ratio	ρ g/cm ³	ρ_f g/cm ³
Sandstone with logging tool	4.0	2.3	1.5	5	10	0.25	2.3	1.0
without logging tool	4.0	2.3	1.5	n/a	10	0.25	2.3	1.0
Granite	5.9	3.4	1.5	2.5	varies	0.25	2.65	1.0
Shale A	2.0	0.8	1.5	5	12.5	0.40	2.3	1.38
Shale B	2.0	1.0	1.5	5	12.5	0.35	2.3	1.38
Shale C	2.0	1.1	1.5	5	12.5	0.30	2.3	1.38

Table 2. Shear velocity based on picks illustrated in Figure 8.

Near Receiver Pick	Far Receiver Pick	Equivalent Shear Velocity in km/s
a. Low Frequency Transducer		
A	A	6.10
B	B	3.39
C	C	3.35
D	D	3.35
E	E	3.31
F	F	3.31
b. High Frequency Transducer		
A	A	5.26
B	B	5.08
C	C	2.88
D	D	4.23
E	E	2.63
F	F	2.93

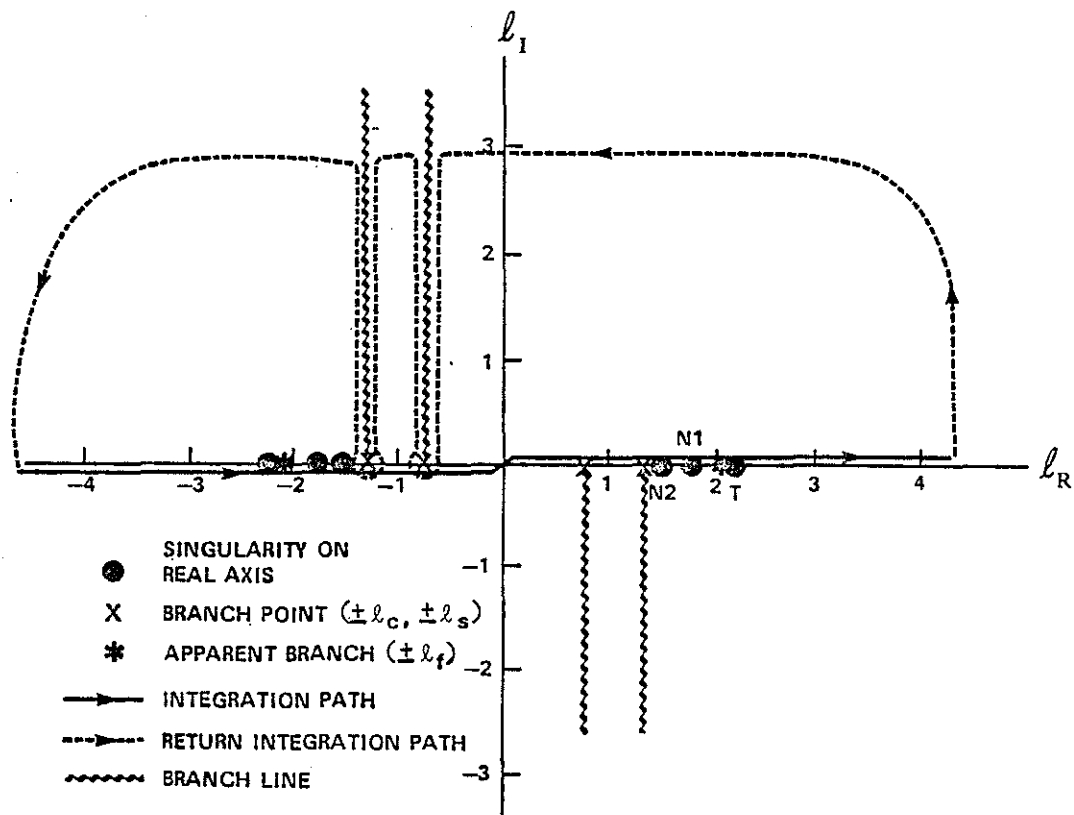


Figure 1. Example of branch cuts and location of singularities for sandstone case at 25 kilohertz using the conventions given by Peterson (1974).

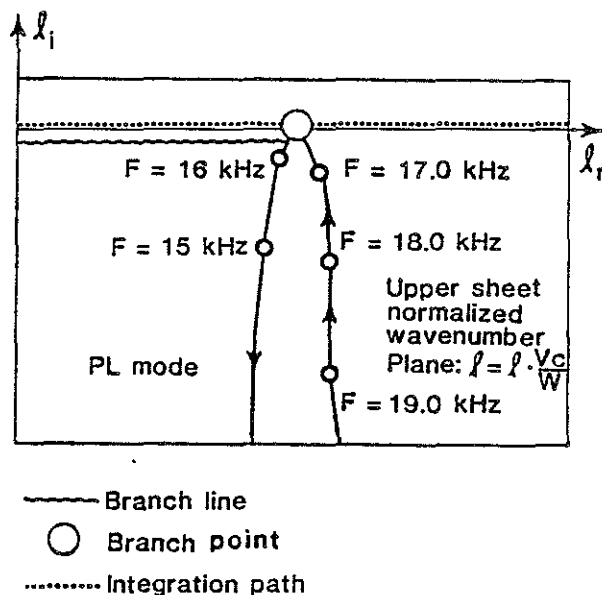


Figure 2. Illustration of trajectory of compressional singularity in the vicinity of mode cutoff; sandstone case with logging tool.

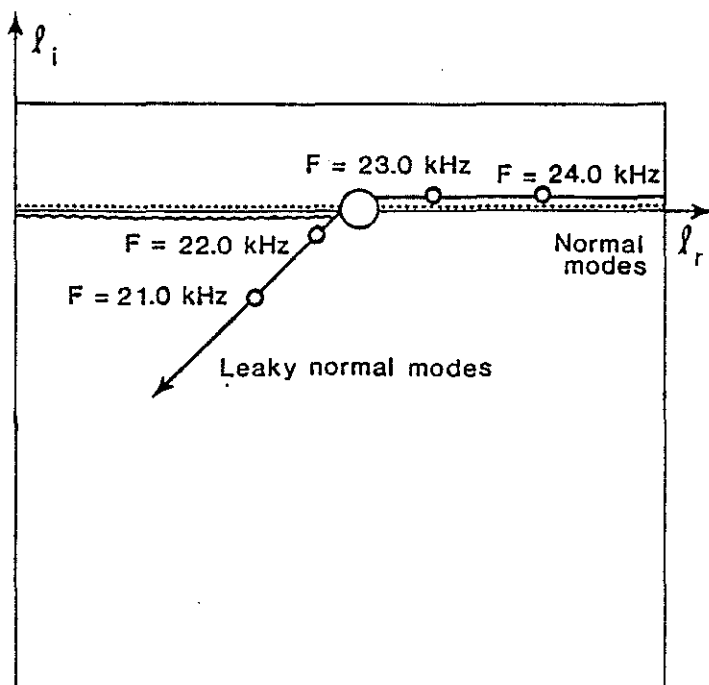


Figure 3. Illustration of trajectory of shear normal-mode singularity in the vicinity of mode cutoff; sandstone case without logging tool.

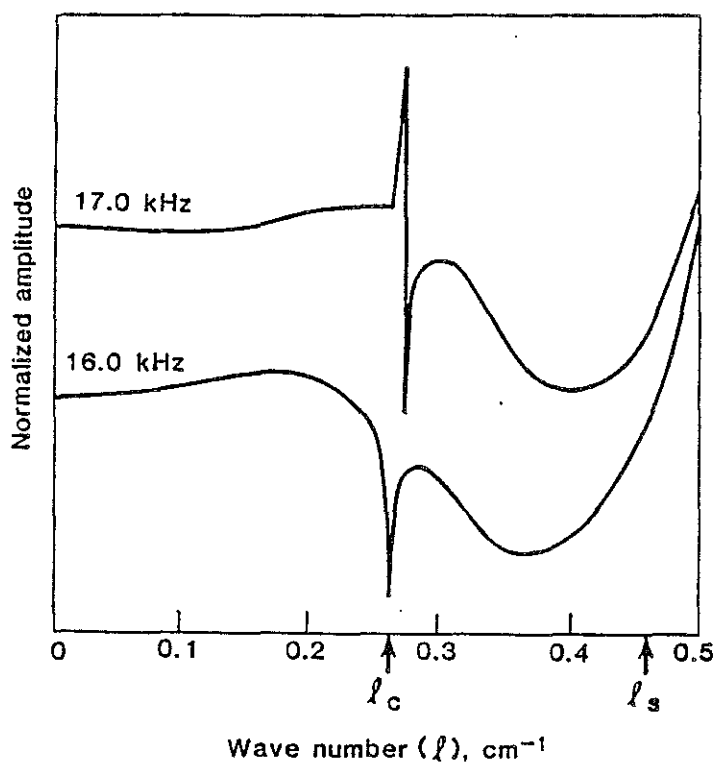


Figure 4. Amplitude of pressure function for wavenumbers near the compressional branch point for frequencies close to compressional normal-mode cutoff- sandstone case with logging tool.

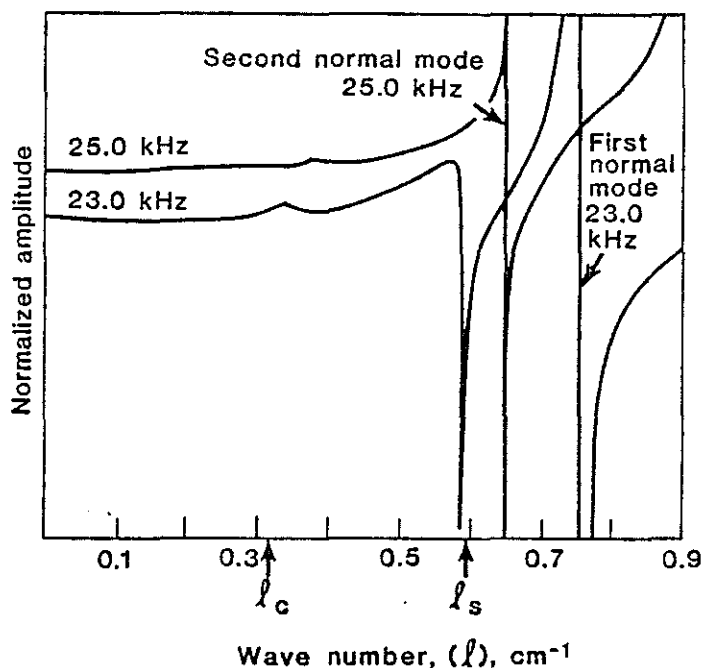


Figure 5. Amplitude of pressure function for wavenumbers near the shear branch point for frequencies close to shear normal-mode cutoff; sandstone case with logging tool.

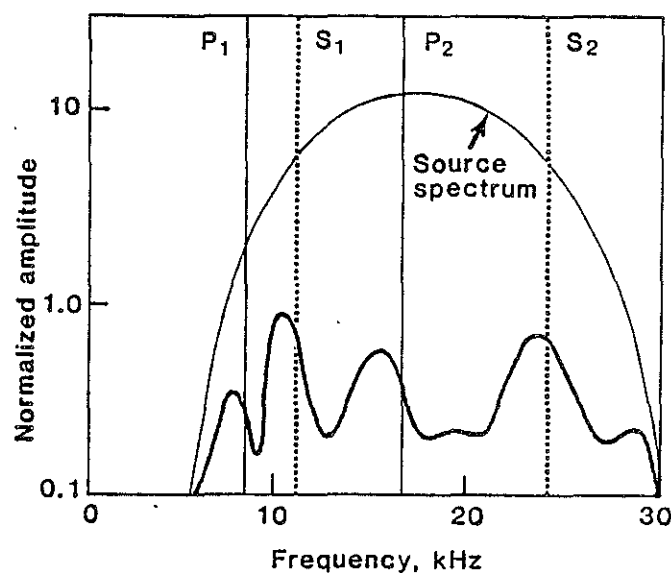


Figure 6. Schematic illustration of head-wave forcing spectrum calculated for broad-band acoustic source; sandstone case with logging tool.

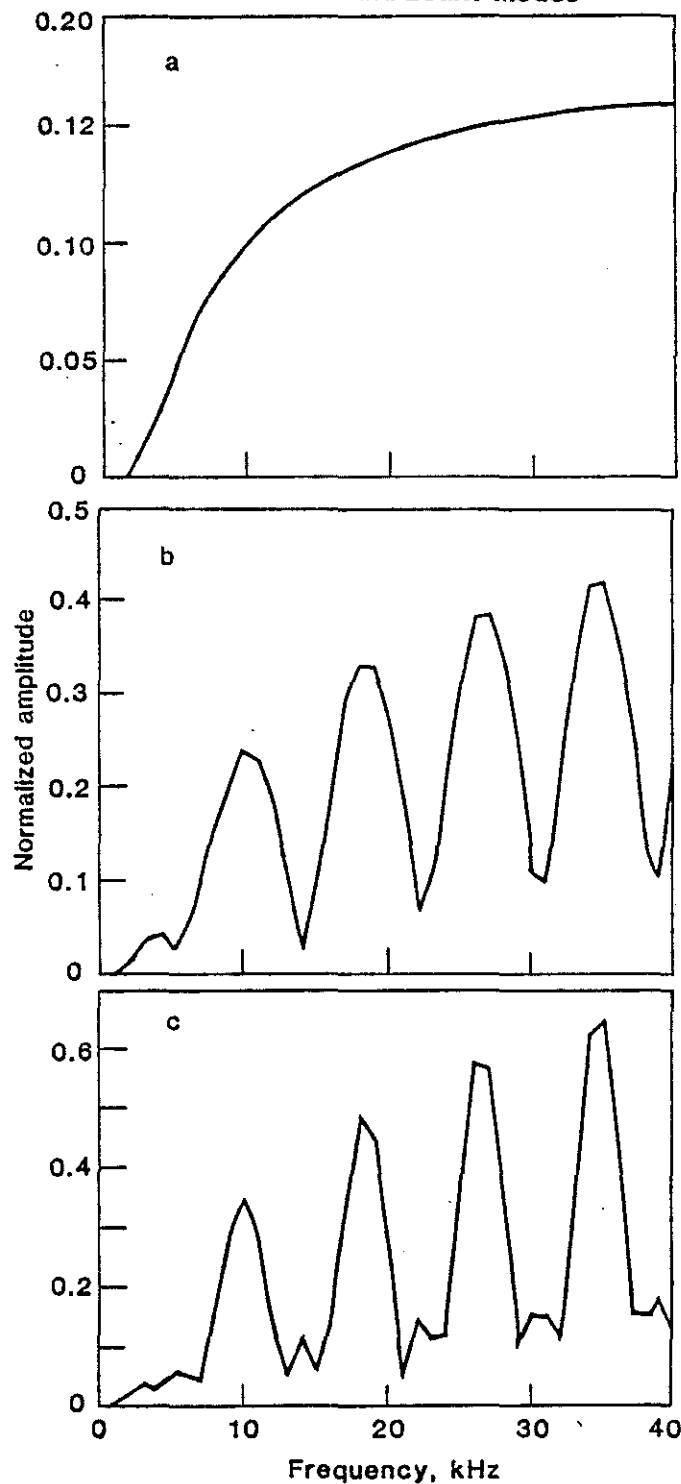


Figure 7. Formal calculation of head-wave spectrum using the Tsang and Rader (1979) branch-cut integration retaining successively higher-order terms in the ray expansion; sandstone case without logging tool.

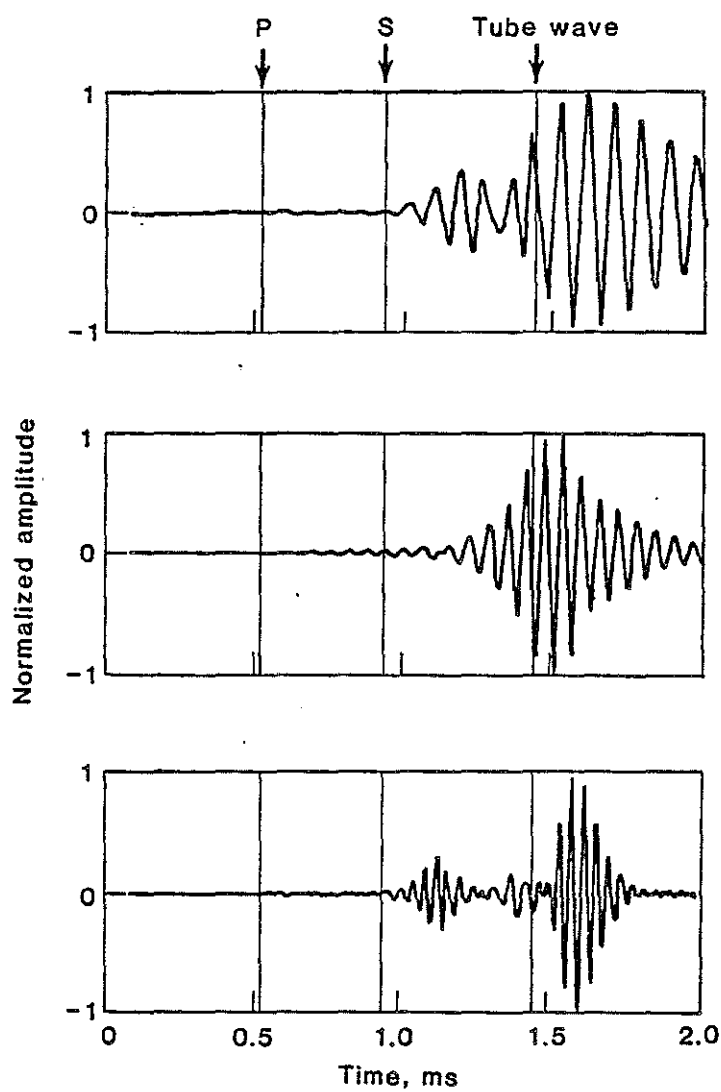


Figure 8. Synthetic seismograms for head waves generated by energy source spanning the cutoff frequencies for (a) first shear normal mode (10 to 11 kHz), (b) first compressional normal mode (16-17 kHz); and (c) second shear normal mode (22-23 kHz); sandstone case.

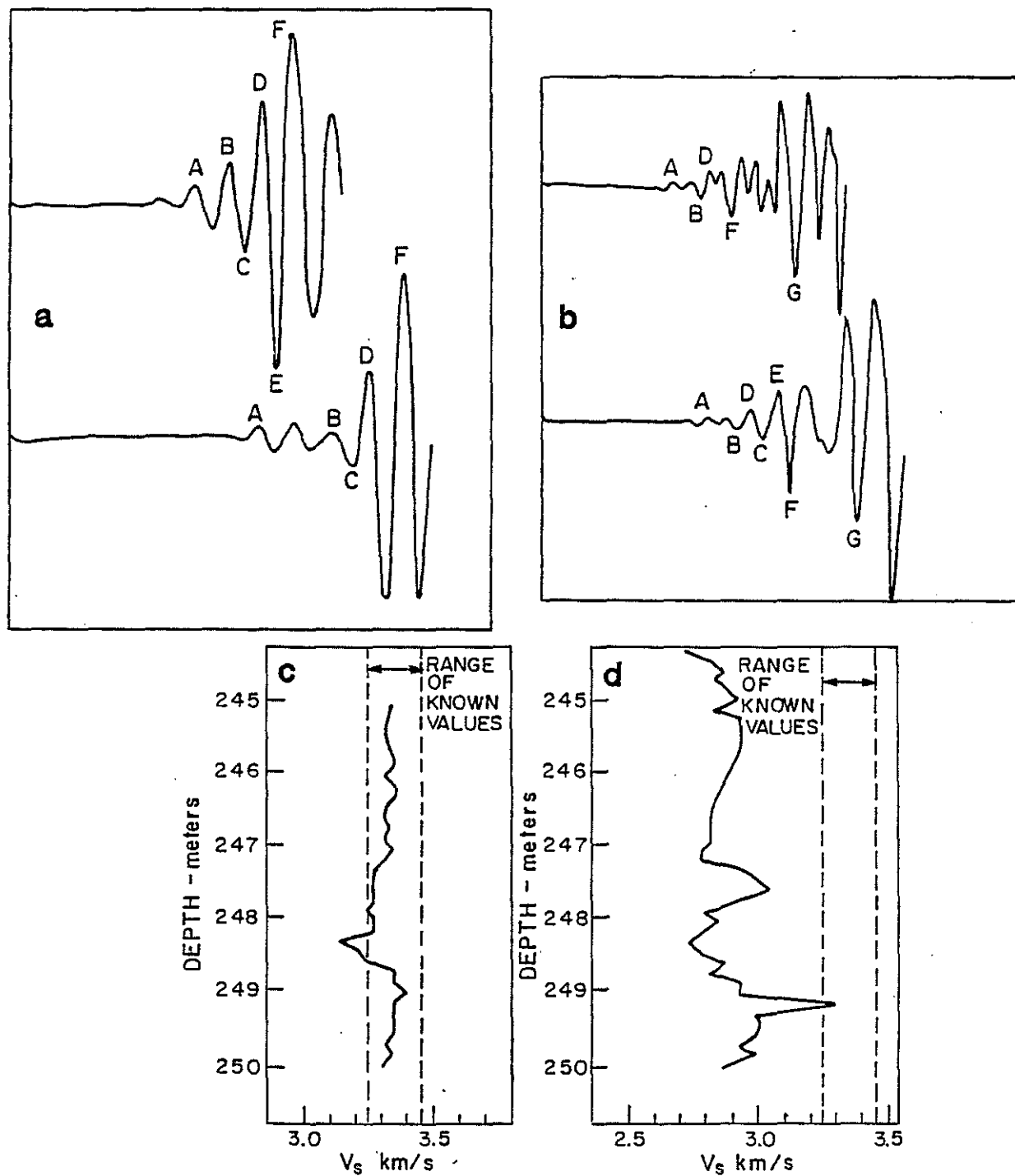


Figure 9. Shear arrival picks at two different source-to-receiver separations for (a) 15 kHz and (b) 34 kHz transducers; and shear velocity picks by the Willis and Toksöz (1983) method (c) 15 kHz and 34 kHz transducers; granite case with 15-centimeter-diameter borehole.

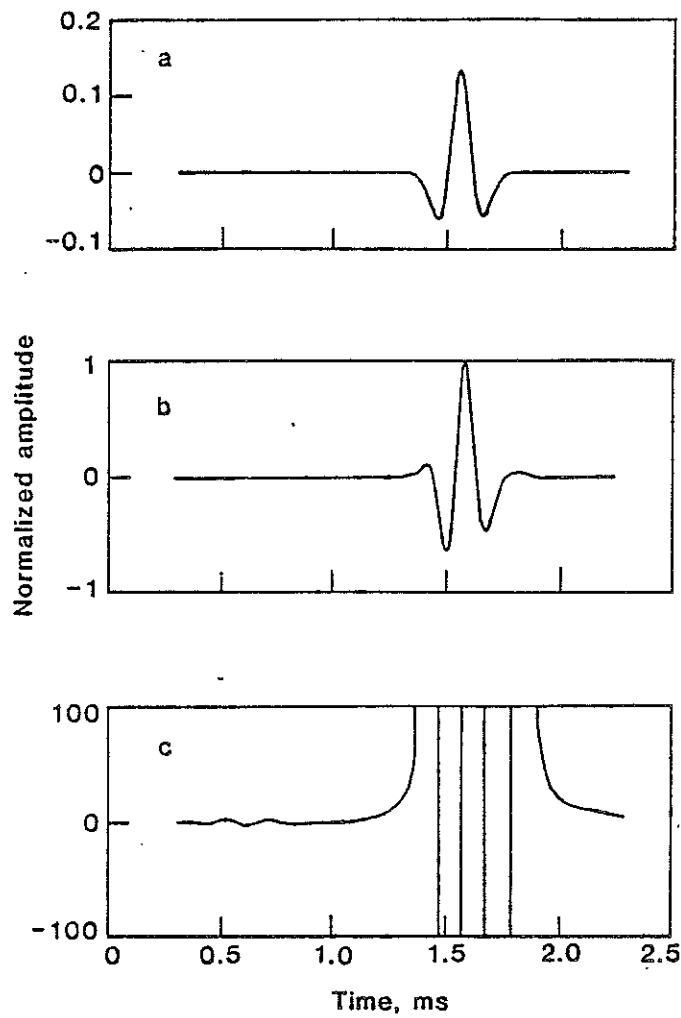


Figure 10. Synthetic waveforms for sources far below cutoff for all modes; (a) source; (b) synthetic waveform for 5-kilohertz source in 8-centimeter borehole; granite case, and (c) expanded waveform illustrating weak compressional arrival.

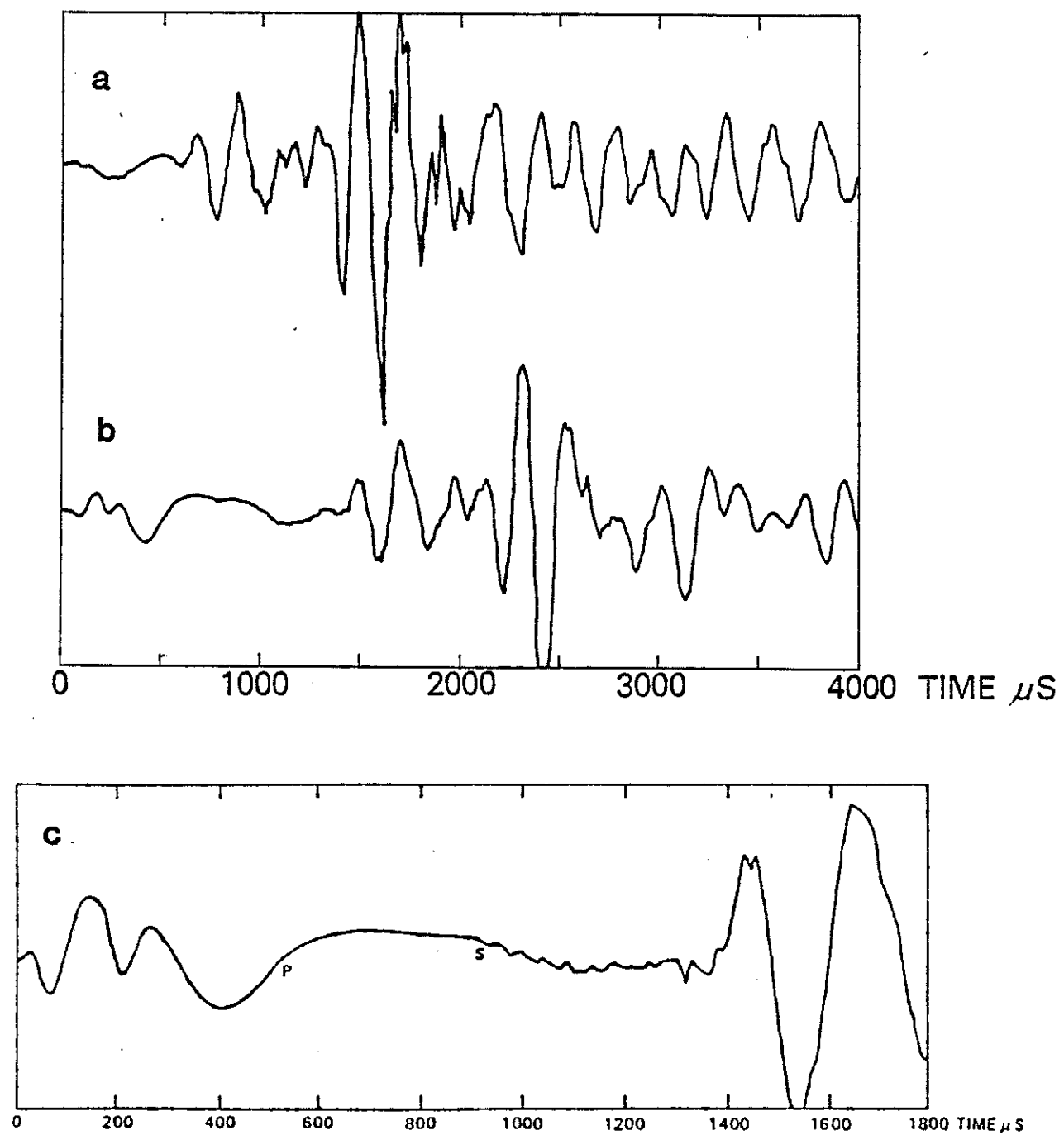


Figure 11. Experimental waveforms obtained in 8 cm diameter borehole at (a) 2 and (b) 2.5 m spacings for 5 kHz source; (c) 2.5 m waveform recorded at higher gain; granite case.

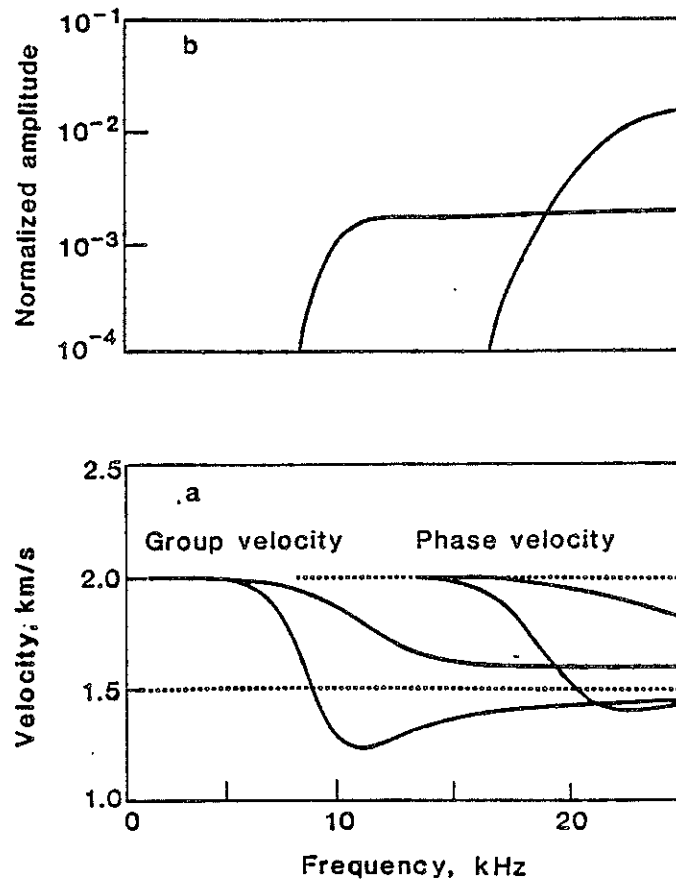


Figure 12. Leaky compressional-mode dispersion for shale "B": (a) group and phase velocities for fundamental and first mode, and (b) amplitude for fundamental and first two modes.

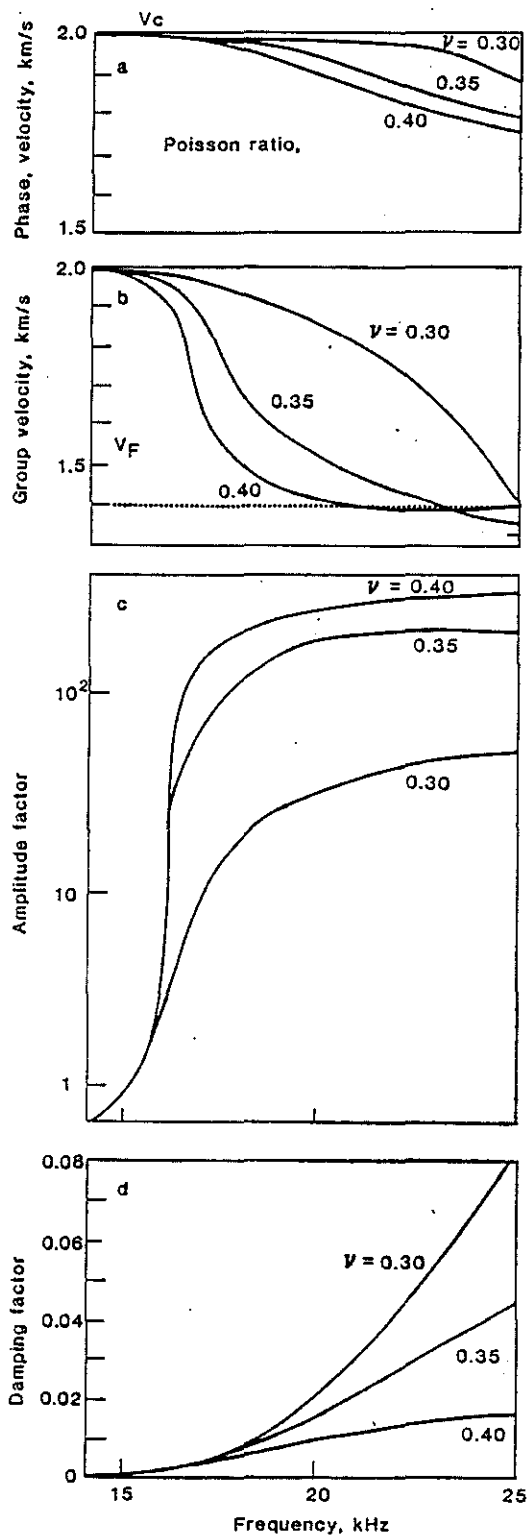


Figure 13. Effect of Poisson ratio on properties of first compressional normal mode; shale "A", "B", and "C".

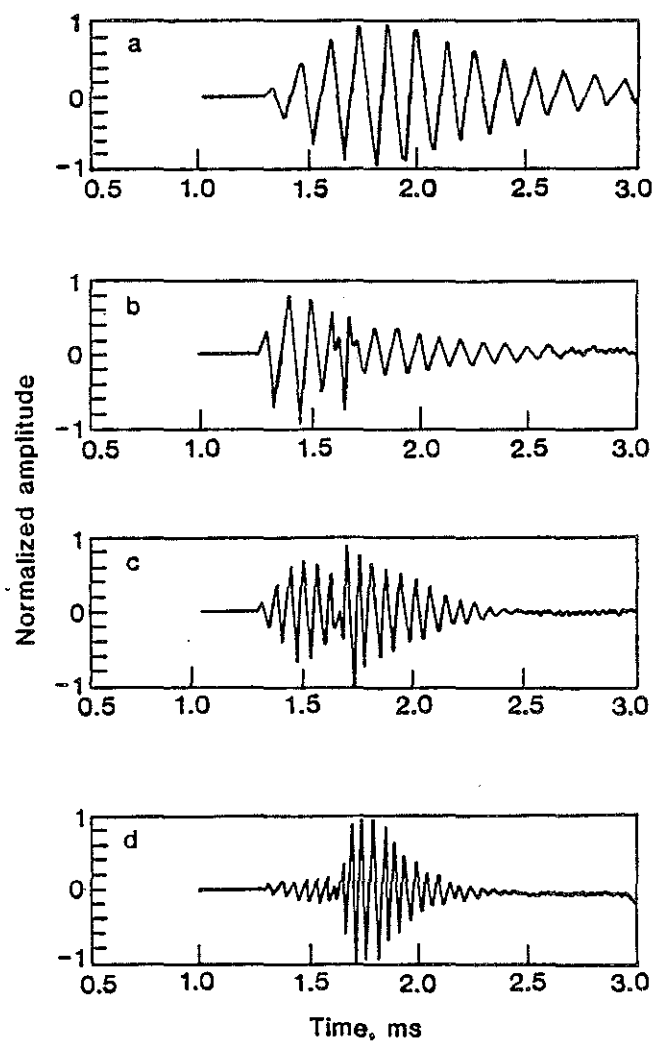


Figure 14. Synthetic waveforms for shale "B" case using narrow band source centered on (a) 7.5 kHz, (b) 10 kHz, (c) 15 kHz, and (d) 20 kHz.

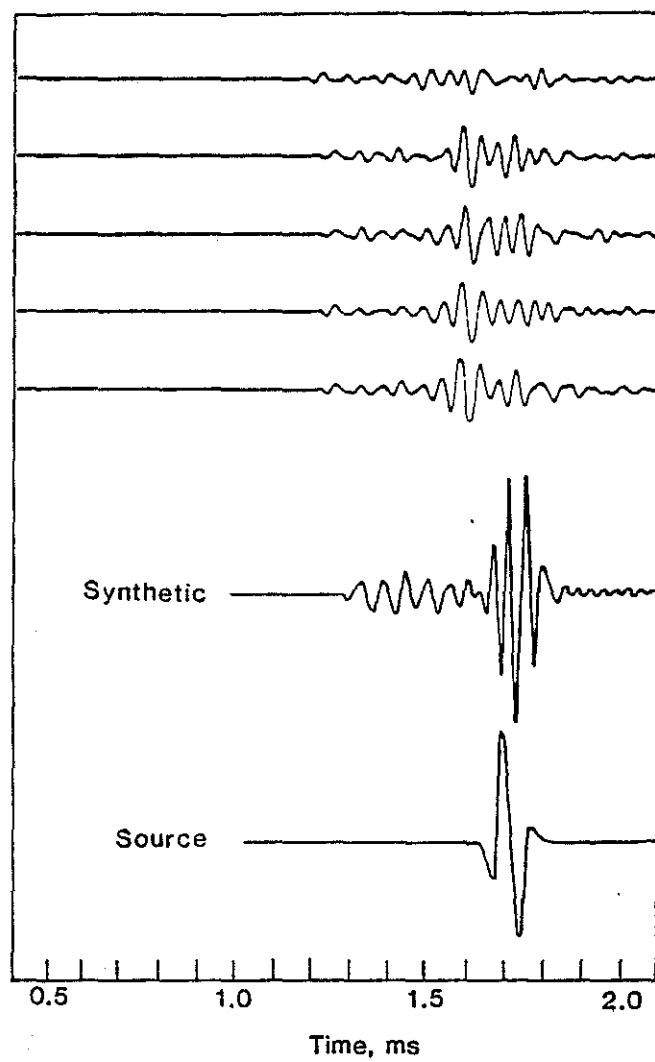


Figure 15. Comparison of synthetic seismograms for shale "B" and broad band forcing 12 kHz with waveforms from argillaceous sea sediments.

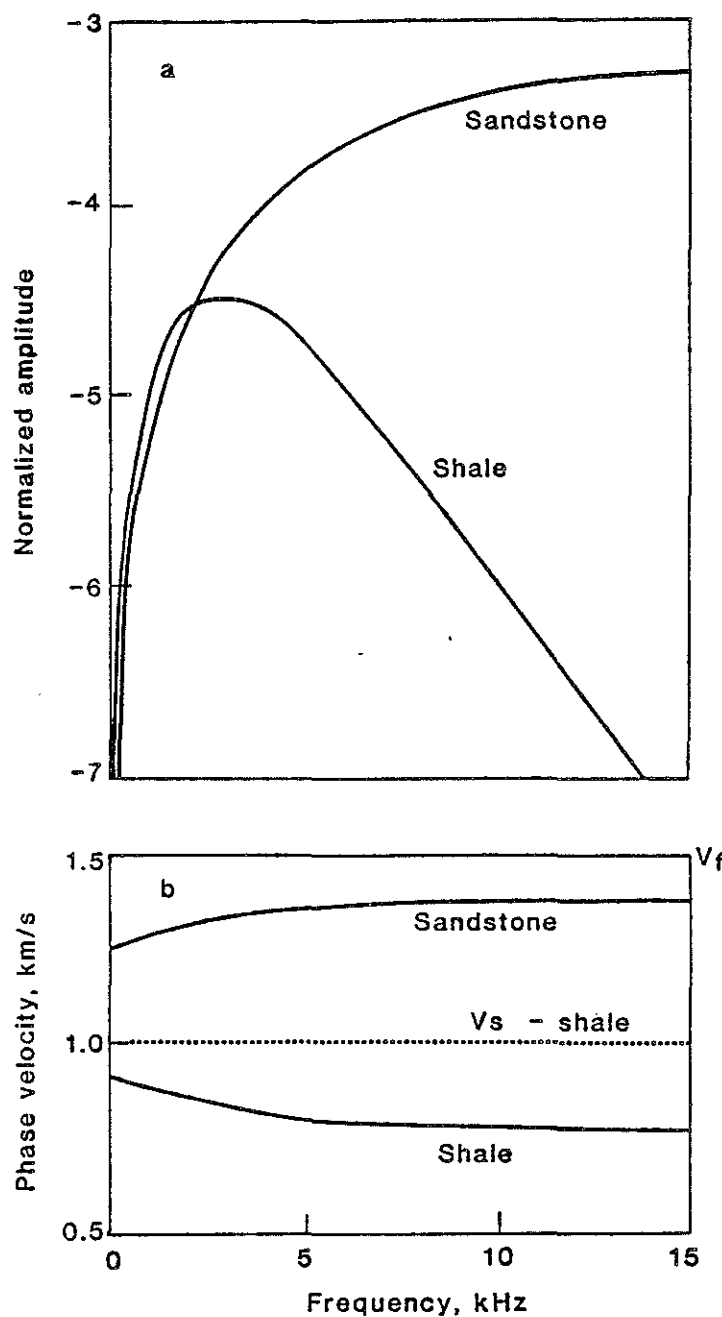


Figure 16. Tube-wave velocities and amplitudes for (a) sandstone case, and (b) shale "B".